J Mater Sci (2014) 49:1812–1823
DOI 10.1007/s10853-013-7869-5

# Dynamics of dysprosium silicide nanostructures on Si(001) and (111) surfaces

**M. C. Zeman · R. J. Nemanich · A. Sunda-Meya**

Received: 25 June 2013 / Accepted: 8 November 2013 / Published online: 26 November 2013


**Abstract** The growth and coarsening dynamics of dysprosium silicide nanostructures are observed in real-time using photoelectron emission microscopy. The annealing of a thin Dy film to temperatures in the range of 700–1050 °C results in the formation of epitaxial rectangular silicide islands and nanowires on Si(001) and triangular and hexagonal silicide islands on Si(111). During continuous annealing, individual islands are observed to coarsen via Ostwald ripening at different rates as a consequence of local variations in the size and relative location of the surrounding islands on the surface. A subsequent deposition of Dy onto the Si(001) surface at 1050 °C leads to the growth of the preexisting islands and to the formation of silicide nanowires at temperatures above where nanowire growth typically occurs. Immediately after the deposition is terminated, the nanowires begin to decay from the ends, apparently transferring atoms to the more stable rectangular islands. On Si(111), a low continuous flux of Dy at 1050 °C leads to the growth of kinked and jagged island structures, which ultimately form into nearly equilateral triangular shapes.

M. C. Zeman
Department of Physics, North Carolina State University, Raleigh, NC 27695, USA

R. J. Nemanich
Department of Physics, Arizona State University, Tempe, AZ 85287, USA

A. Sunda-Meya (✉)
Department of Physics, Xavier University of Louisiana, New Orleans, LA 70125, USA
e-mail: asundame@xula.edu

## Introduction

Rare earth (RE) silicides have been studied extensively on both Si(001) and (111) surfaces for potential use in microelectronics applications. Initially, thin films of RE metals were found to react with Si substrates at temperatures in the range of 300–500 °C to form silicon-rich compounds of the type $RESi_{2-x}$ $(0 < x < 0.4)$ [1, 2]. Investigations into the electrical properties of these silicides revealed Schottky barrier heights of $\sim$0.4 eV on *n*-type Si and $\sim$0.7 eV on *p*-type Si, presenting the materials as good candidates for device applications [3–5]. Furthermore, the epitaxial relationship of the hexagonal $AlB_2$ type structure of many of the RE silicides with Si(111) was found to be $[6]RESi_{2-x}\|[-1-12]Si$ and $(0001)RESi_{2-x}\|(111)Si$, which results in a favorable lattice match between the two materials and offers the opportunity to grow high-quality epitaxial films [7–9].

Lately, interest in RE silicide epitaxy has shifted from the isotropic epitaxial nature of the silicide films on Si(111) to the anisotropic nature of the films on Si(001), as a result of the discovery of a pseudo one-dimensional type of epitaxial nanostructure [6, 10–15]. The growth of high aspect ratio, wire-like nanostructures (nanowires) on Si(001) surfaces, is reported to occur because of strain energy anisotropy brought about by the anisotropic lattice mismatch between the RE silicides and the silicon substrate [6, 16]. Specifically, the epitaxial relationship between the hexagonal form of the silicides and the Si(001) surface is such that the [0001] and $[11\bar{2}0]$ silicide axes are parallel to the $\langle 110 \rangle$ axes of the substrate and $(1\bar{1}00)$ $RESi_{2-x}\|(001)Si$, which is different than that with the (111) surface [8, 17, 18]. In the case of dysprosium silicide, this results in a lattice mismatch with Si(001) of $-0.26$ % in one direction and 7.29 % in the

corresponding orthogonal direction [19, 20]. Therefore, once a nanostructure is nucleated on the surface, growth in the direction of small lattice mismatch does not significantly increase the strain energy, but a significant increase in strain occurs for growth in the direction of large mismatch [6, 21]. This leads to the formation of epitaxial nanowires that grow to microns long in one direction but are only a few nanometers wide in the other. In addition, cross-sectional HRTEM studies have shown that $DyS_2$ nanowires contain one or two layers of hexagonal silicide at the buried interface and two to three surface layers with a faulted stacking that are believed to provide stress relief during growth of the NW islands [20].

The formation of the RE silicide nanowires represents an interesting self-assembled surface phenomenon with the potential to impact the microelectronics industry; however, they appear to be a metastable structure which can only be grown and sustained under certain conditions. The nanowires are typically formed via the deposition of submonolayer amounts of RE metal at temperatures in the range of 500–700 °C. The deposition of excess metal or prolonged annealing at elevated temperatures results in the destruction of the nanowires in favor of larger epitaxial rectangular silicide islands [6, 10, 11, 16, 19, 20]. The mechanisms responsible for the instability of the nanowires are not fully understood. Moreover, the surface evolution of the epitaxial rectangular islands, including stability and coarsening dynamics at elevated temperatures, has not been addressed.

Experimental observations of nanoscale structures usually involve the use of scanning probe techniques such as scanning tunneling microscopy (STM) or atomic force microscopy (AFM). These techniques are capable of high-resolution imaging; however, measurements are usually taken after nanostructure coarsening that has proceeded for a fixed amount of time. In order to fully understand the kinetic and energetic processes that govern the growth and stability of epitaxial nanostructures, an in situ, real-time microscopy technique must be employed.

This study focuses on the growth dynamics of dysprosium silicide nanostructures on Si(001) and (111) surfaces at elevated temperatures. We employ ultra violet photoelectron emission microscopy (UV PEEM) for real-time, in situ observation of the stability and shape evolution of the nanostructures during coarsening. In particular, our results establish that the coarsening of epitaxial $DySi_{2-x}$ islands is strongly influenced by local variations in the size and relative location of the islands on the surface. Additionally, the initiation of a Dy flux during annealing leads to the formation of new $DySi_{2-x}$ nanowires on Si(001) at temperatures above where nanowire growth typically occurs and results in the growth of nearly equilateral nanostructures on Si(111). We find different cross-sectional shapes for the island and nanowire structures on Si(001) and propose that the shape evolution of the nanostructures is related to strain relaxation.

Furthermore, we monitor the decay process of individual wires using real-time photoelectron emission microscopy (PEEM). Direct observation combined with ex-situ AFM measurements is used to analyze the wire growth dynamics, their ordering, shape, and size. Surface ripening is found to occur at the same time as wires and islands are formed. We report on the decay of nanowires and their dependence on their initial width.

## Experimental

All measurements employed $9 \times 9$ mm$^2$ sections of Si(001) (*p*-type, 0.05–0.1 Ω-cm) and Si(111) (*n*-type, 0.05–0.1 Ω-cm) wafers. Prior to loading in UHV, the substrates were cleaned by UV-ozone exposure and a wet chemical etch using a solution of 10:1 hydrofluoric acid diluted in de-ionized water. The substrates were then immediately loaded into ultra high vacuum (UHV) through a load lock and submitted to a thermal treatment at ~950 °C for 15 min. The experiments were performed in a UV PEEM system (Elmitec) with a base pressure $<2 \times 10^{-10}$ Torr. The UV light for the PEEM was generated by the tunable FEL at Duke University with a photon energy range of 3.0–7.0 eV, a Coherent Innova 300 FreD Ar ion laser with a photon energy of ~4.8 eV, or a 100 W Hg discharge lamp with an upper cutoff energy near 5.1 eV. Details of the UV PEEM system have been described previously [22].

The Dy metal was deposited from a four-pocket electron-beam evaporator at temperatures varying from 600 to 700 °C. Thin metal films of ~1–2 nm in thickness were deposited in situ onto the clean substrates at room temperature. After Dy deposition, the samples were annealed to 950–1050 °C to initiate the silicide island formation and growth. The samples were heated in the PEEM system by radiative heating from a tungsten filament in conjunction with electron bombardment directed toward the backside of the sample. The temperature was measured with a thermocouple attached to the sample holder, and the sample surface temperature was calibrated with an optical pyrometer. A potential of −20000 V was applied between the sample and the perforated anode which was ~2–4 mm from the sample surface.

The PEEM images were enhanced with a microchannel plate and displayed on a phosphor screen. All of the images were recorded with a DVC-1312-M-fw digital CCD camera using an exposure time of 3 s. After the growth process, the sample was cooled and removed. Subsequently, a surface morphology analysis was performed using an Autoprobe CP-R atomic force microscope (AFM) in contact

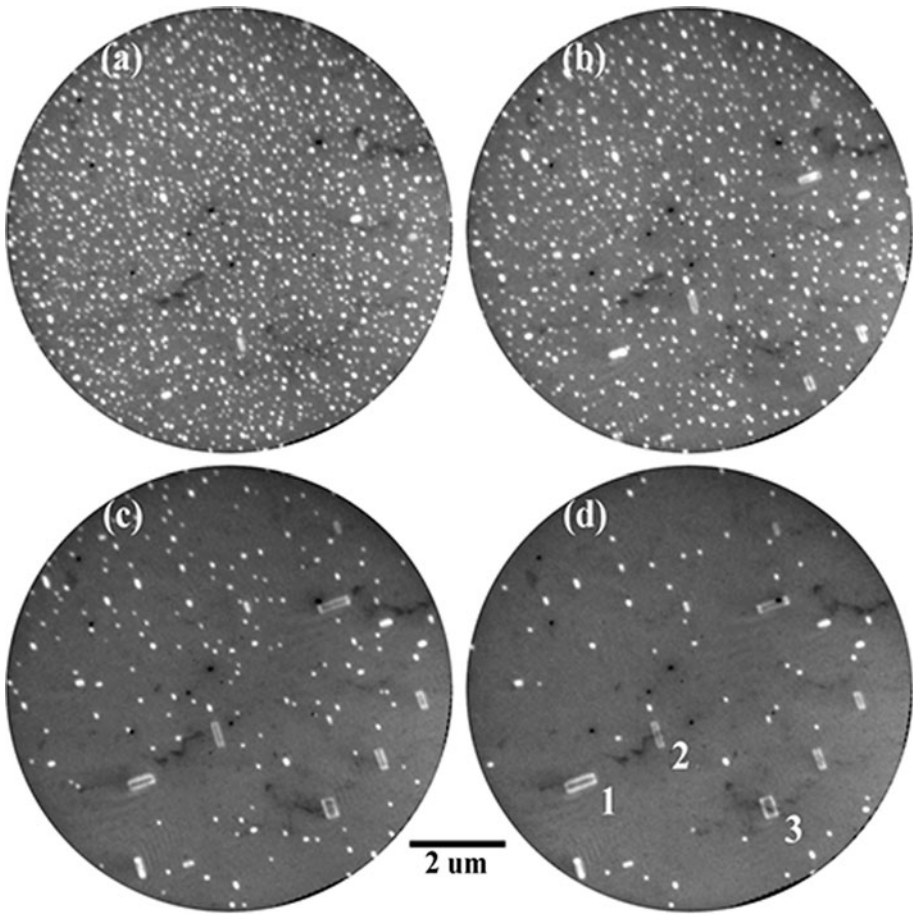


**Fig. 1** A sequence of PEEM images showing a decrease in $DySi_{2-x}$ island density on Si(001) in conjunction with the growth of a few islands during annealing at 950–1050 °C. Image **a** was obtained during annealing the sample at 950 °C for 80 s. Images **b–d** were obtained 5, 275, and 560 s after the sample temperature was increased to 1050 °C, respectively. The field of view of each image is 10 μm. The *dark spots* in the images are defects in the PEEM microchannel plate and are not surface features

mode, utilizing a Si cantilever with a spring constant of 1.6 N/m and a resonant frequency of 170 kHz.

## Results

Prior to depositing the Dy film, the clean Si surface displayed a uniformly dark PEEM image at room temperature. As dysprosium was deposited onto the surface, the PEEM image brightened significantly, indicating increased electron emission from the sample due to the deposition of the low work function metal onto the surface. Once the deposition was terminated, the sample was slowly annealed, and the emission intensity from the surface was observed to decrease due to an intermixing of the Dy overlayer with the underlying Si. Continued annealing to temperatures as high as 1050 °C resulted in the decomposition of the silicide film into 3D nanoscale islands followed by coarsening of the surface nanostructures.

Figure 1 displays a sequence of PEEM images obtained during the annealing of a Dy film which was deposited onto Si(001) at room temperature. The bright white shapes in the images are identified as the $DySi_{2-x}$ islands, and the dark background is the exposed Si substrate. The contrast in the PEEM images is attributed to a difference between the work function of the $DySi_{2-x}$ islands and the photothreshold of the Si substrate. The silicide islands are expected to have a work function that is less than 4.5 eV [2, 23], and the bare Si substrate has a photothreshold of $\sim$5.1 eV [24]. The photon energy of the incident FEL light is tuned to 4.9 eV, which allows for significant electron emission from the silicide nanostructures and nearly undetectable emission from the exposed Si substrate.

During annealing of the silicide island distribution displayed in Fig. 1, images of the surface were recorded every five seconds for the duration of the experiment. As shown in Fig. 1a, the initial $DySi_{2-x}$ island distribution is relatively uniform with most islands being of similar size. As annealing time progresses (Fig. 1b–d), the number of islands on the surface decreases, and a few islands grow larger than the rest. The larger islands develop a distinct rectangular shape indicating they share an epitaxial relationship with the substrate. The areas immediately surrounding the large islands become mostly devoid of smaller nanostructures suggesting that island growth is progressing via atom exchange through surface diffusion, a process often termed as Ostwald ripening [25, 26]. We note that the substrate signal is essentially uniform across each image.

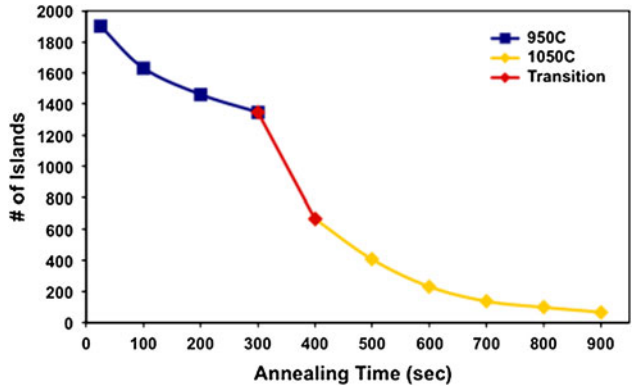


**Fig. 2** The variation in the number of $DySi_{2-x}$ islands during the annealing process shown in Fig. 1

Results have indicated that Dy adsorbed on the Si(100) surface results in a decrease in the work function [27] which could lead to a brighter PEEM image. The uniform substrate signal for each image suggests that either the PEEM at this wavelength is not sensitive to the change in work function and/or that the Dy atoms are uniformly distributed across the surface.

Figure 2 displays the change in the number of islands in a 10-μm field of view with annealing time. As the sample temperature reached 950 °C, there were ~2000 islands in a ~78.5 $\mu m^2$ area of the surface. Continued annealing at 950 °C for 300 s resulted in a reduction of the number of islands to ~1350. The sample temperature was then increased to 1050 °C, and the island ripening rate increased significantly; this increase is reflected as a sharp drop in the number of islands on the surface as seen in the "transition" portion of the graph in Fig. 2. After the temperature was stabilized at 1050 °C, the number of islands continues to decrease at a decreasing rate for the remainder of the annealing cycle.

The growth and shape evolution of the island labeled number 1 in Fig. 1d is displayed in Fig. 3. In Fig. 3a the island has been annealed at 950 °C for ~80 s. The nanostructure is compact with an elongated shape, measuring 184 nm long and 102 nm wide. After annealing at 950 °C for a total of 300 s (Fig. 3b), the overall size of the island has increased, with the length increasing by 75 nm and the width increasing by 20 nm. The number of smaller surrounding islands has decreased in conjunction with this size increase, suggesting that they are decaying and supplying material to the larger island to sustain its growth (Ostwald ripening). Evaporation of the Dy also contributes to the reduction of the island density. As the temperature is increased to 1050 °C, the rate of island growth accelerates. After annealing at 1050 °C for 185 s, the island length has reached 496 nm, and the width is 223 nm (Fig. 3c). After 560 s at 1050 °C, all of the surrounding small compact nanostructures have disappeared, and the island has

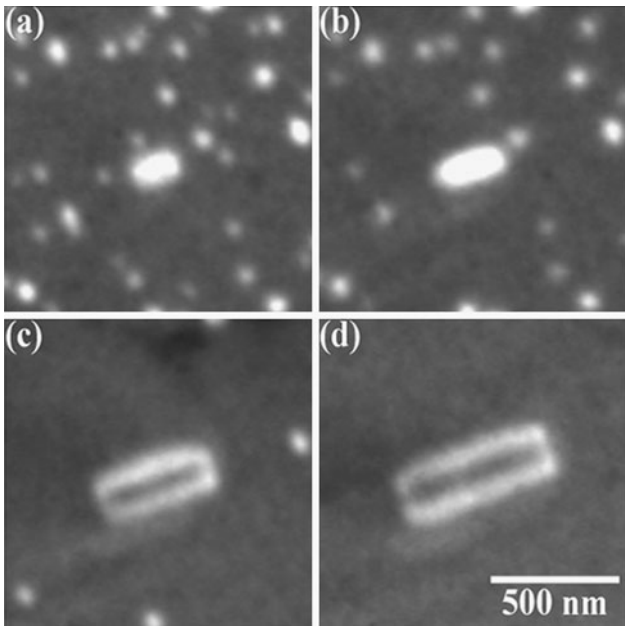


**Fig. 3** A sequence of PEEM images showing the growth of the $DySi_{2-x}$ island labeled number 1 in Fig. 1d. Images **a**, **b** were obtained during annealing at 950 °C for 80 and 300 s, respectively. Images **c**, **d** were obtained 185 and 560 s after the sample temperature was increased to 1050 °C, respectively

reached a length of 658 nm and a width of 263 nm (Fig. 3d). Furthermore, larger islands in Fig. 3c and d show a decrease in contrast when compared to smaller structures in (a). This change may be partially due to a change of crystal structure for the surface layer and/or a decrease in work function due to electron confinement as the structure height approaches the Fermi wavelength [28].

When we deposit just a few monolayers of Dy at ~700 °C, a very dense array of narrow nanowires are formed (Fig. 4). They measure up to ~0.5 μm in length and ~10 nm in width. The nucleation of these wires occurs too rapidly to be observed with the PEEM. Their growth appears to stop only when they intersect another wire. They have a more uniform morphology and size distribution, while they populate the entire surface. Immediately following the formation of the new structures, the nanowires begin to decay (Fig. 4b–f). When annealed at 750 °C, they decay more rapidly than the wider wires. They shrink from the ends before completely disappearing. Starting from Fig. 4c, empty areas that were occupied by the nanowires appear on the surface. Since additional nucleation is not observed during the entire decay process, and no structure seems to increase its size; evaporation seems to be an important mechanism of nanowire decay. We note that diffusion of Dy into the bulk is less likely to affect the size distribution. The typical solid solubility limit of transition metals in Si is between $10^{-7}$ and $10^{-9}$ at 1000 °C [29]. For RE metals such as Er in Si, a solubility of $1 \times 10^{16}$ $cm^{-3}$ has been reported

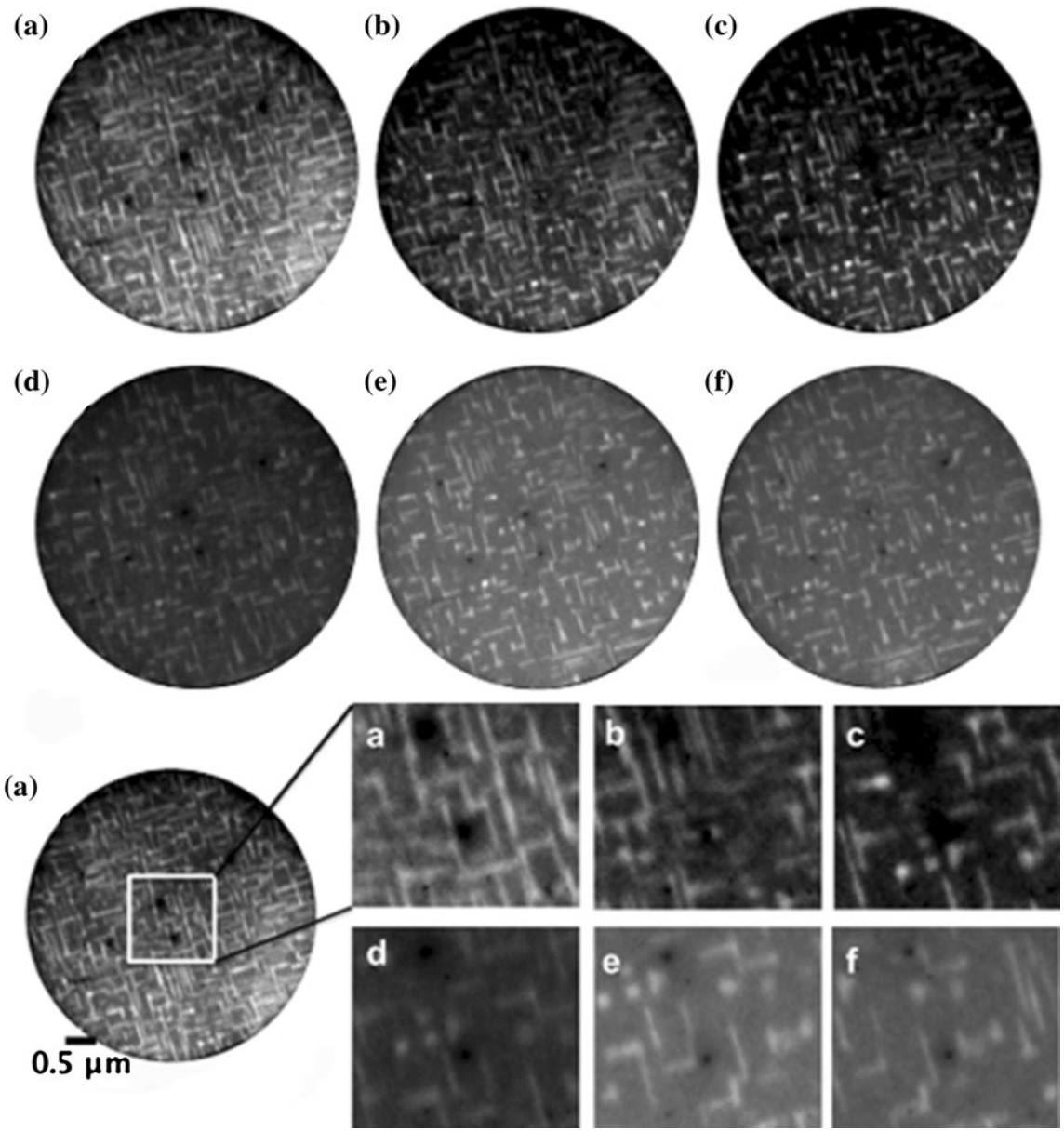


**Fig. 4** A sequence of the decay of narrow wires (length up to 0.5 μm, width ~10 nm) formed after deposition of a few monolayers of Dy at 700 °C. The sample temperature was subsequently raised to 750 °C: **a** nanowires array as formed, **b** after 60 s, **c** 132 s, **d** 192 s, **e** 246 s, and **f** 288 s (FOV: 5 μm)

at 1300 °C [30], and an area concentration limit of (2.0–5.0) × $10^{11}$ $cm^{-2}$ was found for ion implanted Si after annealing to 900 °C [31]. These results suggest that less than a monolayer of Dy could be accommodated in the bulk.

Figure 5a shows a PEEM scan of $DySi_2$ nanowires array formed after the deposition of few monolayers. Figure 5b displays AFM images for typical nanowire and island structures. The plain cleaned substrate was heated at 675 °C before depositing Dy for ~3 min. Nanowires are formed after annealing at 675 °C for 3 min. The nanowires grow along one of the two $\langle 110 \rangle_{Si}$ orthogonal directions, with no apparent preference for either orientation. This result is likely related to the presence of multiple domains on the surface. They exhibit high length-to-width ratios, and a line profile of the wires (taken perpendicular to their long direction) indicates sloped sides (Fig. 5c). They do not appear to cross each other but end or start at the intersection point. They measure up to ~2.5 μm in length, with a width between 60 and 80 nm and an average height of ~4.0 nm.

Similar to the experiments on Si(001), $DySi_{2-x}$ islands were grown on Si(111) by first depositing 1–2 nm of Dy onto a clean substrate at room temperature. Following the deposition, the sample was slowly annealed to 950 °C. During the temperature increase, the emission from the

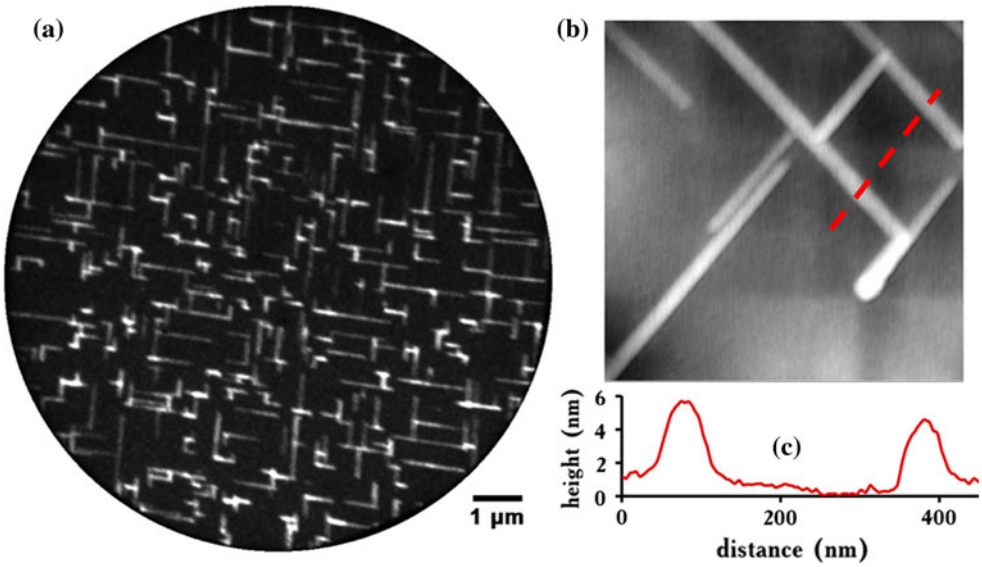


**Fig. 5** **a** A PEEM scan of $DySi_2$ nanowires array formed after the deposition of few monolayers at 675 °C, followed by annealing at 675 °C for 3mn; **b** Ambient AFM 1 × 1 $\mu m^2$ viewgraph; **c** line scan over two wires: *triangular*-shaped nanowires are aligned in two preferential directions. They measured up to ∼2.5 μm in length with a width of 60–80 nm and a height of ∼4 nm

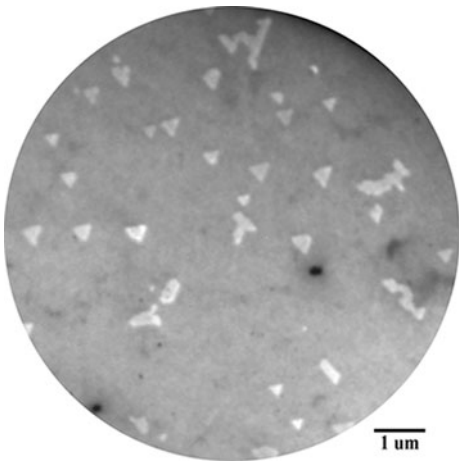


**Fig. 6** A PEEM image acquired at room temperature showing the distribution of $DySi_{2-x}$ islands on Si(111) after annealing at 950 °C for 300 s. The field of view of the image is 10 μm. The *dark spots* in the images are defects in the PEEM microchannel plate and are not surface features

surface was observed to decrease (signifying silicide formation), and the film broke up into island structures. Once 950 °C was reached; the sample was annealed for 300 s, and very little island coarsening was observed. Figure 6 displays a PEEM image of the sample after a quench to room temperature following the 950 °C anneal. The sample contains many islands that roughly resemble equilateral triangles with sides ranging from 220 to 450 nm in length. There are also other island structures, some of which have faceted edges running in the same directions as the triangles, and others that have less defined edges.

Following the temperature quench, the sample was re-annealed to 1050 °C. Figure 7 focuses on a single large faceted island and several nearby smaller islands during this annealing process. Figure 7a, b displays the group of islands after annealing at 1050 °C for 105 and 290 s, respectively. When the temperature initially reached 1050 °C, the small islands were all roughly triangular in shape. As the annealing progressed for 105 s (Fig. 7a), the triangular islands began to lose their shape and are reduced in size. After 290 s (Fig. 7b), the small islands have almost completely disappeared, and some of the kinks in the larger island have been filled in. This suggests that as the smaller islands decay, Dy atoms detach and diffuse across the surface to be incorporated into the larger island. After annealing for a total of 300 s, a slow, steady deposition of Dy was initiated.

The deposition of Dy at 1050 °C lasted for ∼15 min. Figure 7c, d shows the growth of the large island as a result of this deposition. After 270 s of deposition, two edges of the island have become straight and kink-free (Fig. 7c). Continued deposition for another 290 s resulted in the growth of the third island edge leading to a nearly equilateral structure with the average length of each side being ∼1000 nm. Interestingly, significant growth of the small nearby island was not observed; this suggests that the deposited Dy atoms were diffusing on the surface and preferentially attaching to the larger island. No new islands were nucleated during this process.

## Discussion

The driving force for the formation of the island structures in Fig. 1 is the equilibrium among the surface and interface energies of the initially formed $DySi_{2-x}$ film and the silicon substrate. Prior studies by Travlos et al. [32] have shown that $DySi_{2-x}$ forms from a Dy film on silicon at temperatures as low as 300 °C. As the $DySi_{2-x}$ film is annealed to higher temperatures, sufficient thermal energy is supplied to the system allowing the surface free energies of the film

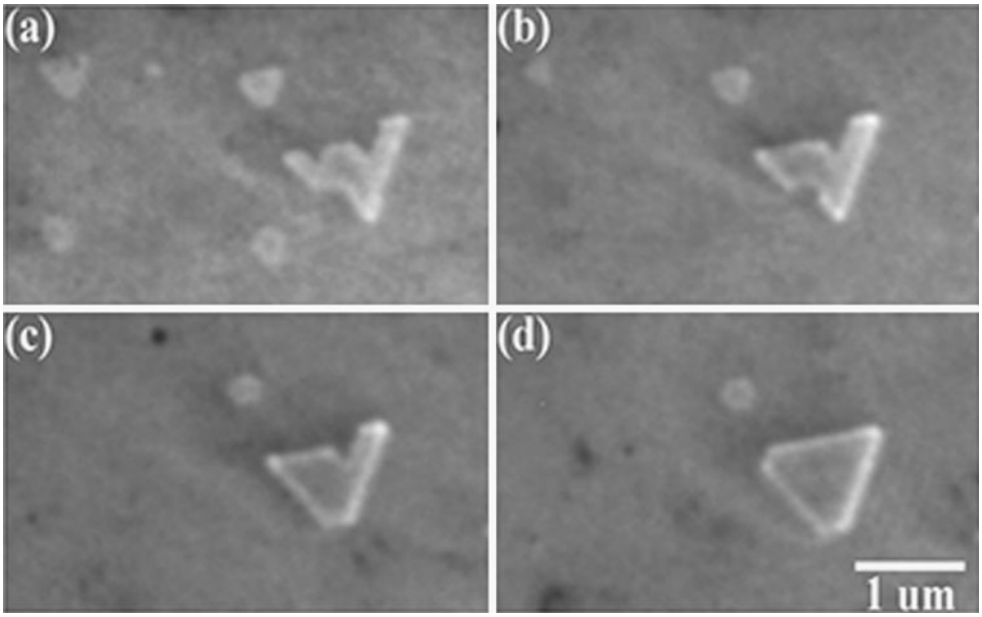


**Fig. 7** A sequence of PEEM images showing the growth of a $DySi_{2-x}$ island on Si(111) during annealing at 1050 °C. Images **a**, **b** were obtained after annealing at 1050 °C for 105 s and 290 s, respectively. Images **c**, **d** were obtained during the deposition of Dy metal at 1050 °C for 270 and 560 s, respectively

and substrate to reach equilibrium with the free energy of the interface between them. In general, the surface with the highest energy will be minimized, which affects the morphological characteristics of the system and determines whether the film will wet the surface or form islands. In the case of $DySi_{2-x}$ on Si(001), the result is the formation of nanoscale silicide islands and wires [15, 32–37]. Other effects, such as interface bonding, strain, and kinetics, will also influence the formation and morphology of the islands [15, 32]. In addition, mobility has been shown to be a driving mechanism for the formation of highly elongated islands [14], and the different crystal structures have been associated with larger islands of compact or nanowire morphology [34, 35].

## Nanostructure Coarsening

As the initial island distribution in Fig. 1a is continuously annealed at elevated temperatures, some of the nanostructures grow at the expense of others (Fig. 1b–d). The larger islands in the distribution grow and many of the smaller islands shrink and eventually disappear. This phenomenon, known as Ostwald ripening, is described by the Gibbs–Thompson (G–T) relation, [25, 26, 38]

$$C_{\mathrm{r}} = C_{\infty} e^{2\gamma\Omega/rkT}, \quad (1)$$

where $C_{\mathrm{r}}$ is the adatom concentration at the perimeter of an island, $C_{\infty}$ is the equilibrium adatom concentration of an island of infinite radius ($r \to \infty$), $\gamma$ is the surface energy per unit area of the island, $\Omega$ is the volume occupied by one formula unit of silicide, $k$ is the Boltzmann constant, and $T$ is the absolute temperature. The adatom concentration $C_{\mathrm{r}}$ will vary with island dimensions. Large islands will have a lower surrounding adatom concentration than smaller islands; consequently an adatom concentration gradient will develop between islands of different sizes. This concentration gradient drives the diffusion of adatoms from small islands to large islands resulting in the island growth shown in Fig. 1.

Interestingly, we observe that larger faceted islands in Fig. 1d grow at different rates during annealing at 1050 °C. Over the course of the annealing cycle shown in Fig. 1, the growth of the three numbered larger islands is characterized by their lengthening and change in length-to-width ratio, $l/w$. Island 1 lengthens by 70 % and $l/w$ changes from 2.1 to 2.5, island 2 lengthens by 33 % and $l/w$ increases from 2.6 to 3.1, and island 3 lengthens by 47 % and $l/w$ changes only from 1.7 to 1.6.

The elongation of the islands is possibly due to several effects. A model proposed by Jesson et al. [39] suggests that island elongation is due to a kinetic instability leading to facet growth. In this model, the growth of the end facets is faster than the edge facets due to strain energy considerations. Therefore, any residual strain energy in the $DySi_{2-x}$ islands could lead to an increase in island length. Alternatively, Fitting et al. [40] proposed that strain relaxation may drive the elongation of the islands. Their model suggests that the misfit structure of an island will define its shape, and the island will grow longer along the dislocation direction. Kastner and Voigtlander [41] have

employed the energy barrier to explain the island elongation: as a faceted island grows, the adatoms which attach to the edges of the islands will diffuse to the ends because the energy barrier for the nucleation of a new atomic layer on a facet is larger at the edges. Shinde et al. [15] explain the orientation of disilicide nanowires on Si(001) as a result of a preference for adatoms to form atomic chains perpendicular to Si dimer rows on the clean Si(001) surface, and these atomic chains are precursors to nanowires.

The exact mechanism responsible for the island elongation remains unclear; however, the differences in the overall island growth rates may be attributed to variations in the island distributions that surround each of the growing nanostructures. The adatoms that sustain the growth of the larger islands during coarsening originate from the smaller surrounding nanostructures, so the size and location of the surrounding structures will significantly affect the evolution of the larger growing islands [25, 26].

To investigate these variations, an ensemble of islands was observed during Oswald ripening. The larger nanostructures grow larger, and the smaller nanostructures shrink away and disappear. However, for islands with areas between 0.005 and 0.01 $\mu m^2$, it appears that they have an equal chance to grow or to decay. Figure 8 shows three different islands at the center of a $\sim$1.5 μm radius area of the surface: island 1 is in Fig. 8a, island 2 in Fig. 8b, and island 3 in Fig. 8c. The sizes of the largest nearby nanostructures are indicated in the images. Figure 8a shows island 1 surrounded by many islands of moderate size; however, none are larger than it. Therefore, island 1 grows via Ostwald ripening at the expense of the surrounding structures. Similarly, island 2, shown in Fig. 8b, is the largest structure in its immediate vicinity. It grows initially and remains relatively stable throughout the remainder of the annealing cycle (the slight reduction in size may be due to evaporation). Interestingly, island 1 reaches a much larger final size than island 2. This can be attributed to the fact that island 1 is surrounded by a higher density of larger nanostructures compared to island 2, which would provide more adatoms to sustain its growth. Finally, island 3 is close to two islands (both to its left, the 0.142 and 0.154 islands) that are significantly larger than it. Thus, island 3 decays at the expense of the larger islands. From these observations, it is apparent that island size and location play a major role in determining the evolution of the island distribution.

The growth rates for islands 1 (initially 0.0080 $\mu m^2$), 2 (initially 0.0080 $\mu m^2$), and 3 (initially 0.0081 $\mu m^2$) are plotted in Fig. 9. Although these islands are initially similar in size, island 1 grows significantly, island 2 grows initially then shrinks slightly but remains stable, and island 3 decays and disappears rather quickly. Since the density of nanostructures in the immediate vicinity of each of these islands is similar, the difference in their observed coarsening behavior must be understood by considering the size of the surrounding nanostructures. A similar study by Bartelt et al. [42] reported on the ripening of two dimensional silicon islands on Si(001).

The cross-sectional profile of the nanowires suggests that strain plays a dominant role in determining the shape of the nanostructures. In a system such as $DySi_{2-x}$/Si(001) where a significant lattice mismatch exists between the silicide nanostructures and the underlying substrate, dislocation-induced strain relaxation will strongly influence the shape evolution of the structures. Initially, for a growing nanostructure, an increase in height will contribute to strain relaxation because the strain energy density decreases from the island/substrate interface to the island peak [39, 43]. Thus, the nanostructure will grow by increasing its vertical aspect ratio resulting in the formation of an overall triangular cross-section. The nanowires shown in Fig. 5 exhibit sloped sides which could reflect this effect. As the nanostructure continues to increase in volume, it will eventually grow beyond a critical thickness where it can no longer accommodate the increasing elastic strain energy and a misfit dislocation will form to relieve the elastic energy of the island [44]. The introduction of the dislocation leads to the lateral expansion of the nanostructure. This process of dislocation nucleation and lateral expansion lowers of the vertical aspect ratio of the island, leading to a flattening of the island's top surface. The PEEM images in Fig. 3 indicate that the largest islands tend to have flat surfaces. Similar shape change effects have been observed for erbium silicide nanostructures on Si(001) [16] and for nanoscale $TiSi_2$ islands on Si(111) [44, 45].

## Decay of $DySi_{2-x}$ nanowires on Si(001)

The nucleation of the nanowires shown in Fig. 4 occurs too rapidly to be observed with the PEEM. Their growth appears to stop only when they intersect another wire. They have a more uniform morphology and size distribution, while they populate the entire surface. Under continuous annealing, they shrink from the ends before completely disappearing. Since additional nucleation is not observed during the entire decay process and no structure seems to increase its size, evaporation seems to be an important mechanism of nanowire decay.

One nanowire was chosen and measured during the entire decay process to have a hint on the decay mechanism. Its length is plotted as a function of time in Fig. 10. Its decay is almost linear with time. When the nanowire size reaches about 20 % of its initial size, an abrupt transition in decay rate was observed.

$DySi_2$ nanowires appear to grow and decay in length, while the width stays constant. They aggregate adatoms preferentially from the ends rather than from their straight

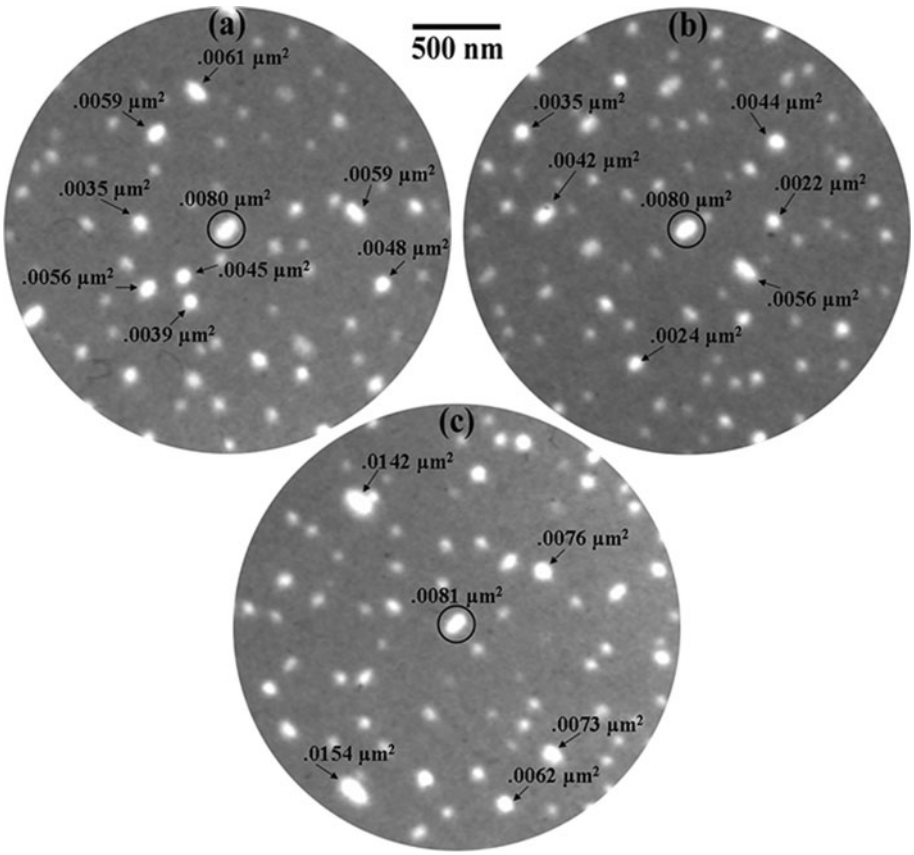


**Fig. 8** Initial PEEM images of three different islands on a Si(001) surface; each at the center of a ~1.5 μm radius area of the surface. Island 1 is in (**a**), island 2 in (**b**), and island 3 in (**c**). The size of other large nanostructures is indicated in the images with different distributions of nearby islands grown on a Si(001) surface. For each central island the change in area with time is presented in Fig. 9

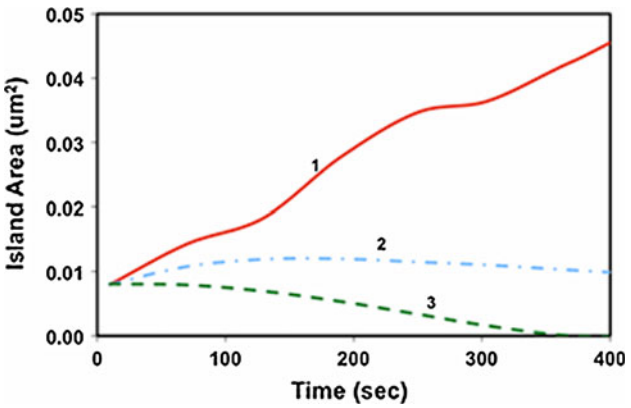


**Fig. 9** Growth rates during annealing at ~1000 °C for islands *1* (initially 0.0080 μm$^2$), *2* (initially 0.0080 μm$^2$), and *3* (initially 0.0081 μm$^2$) from Fig. 8

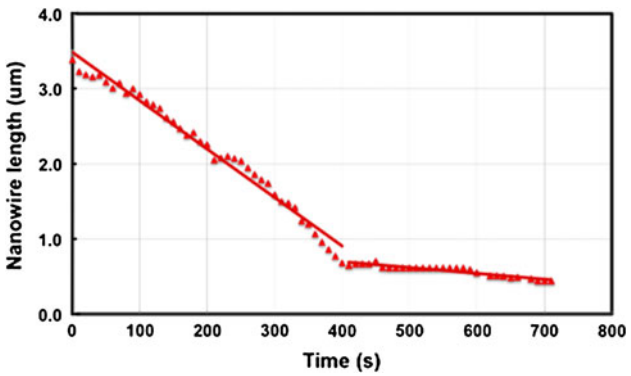


**Fig. 10** The initial decay seems to be linear with time. An abrupt transition in the decay rate is observed when this nanowire reaches about 20 % of its initial size

edges. Further diffusion of the dysprosium around the edges and through the bulk increases the width of the nanowires. The extrinsic stress (due to the change in temperature) and the intrinsic stress (due to molar volume evolution or relaxation) combine to give the nanowires their final shape.

When the Dy flux stops, a ripening process takes place due to coarsening kinetics as annealing proceeds. The excess Dy deposition over a few monolayers gives rise to thick and sparse nanowires. We suggest that because a greater amount of Dy is available on the surface, Dy can diffuse with less energetics cost to join a nanowire. Such an easier transport will allow the $DySi_2$ to coarsen into fewer and larger nanowires. Further annealing during this heteroepitaxial growth induces the instability of the surfaces, which is caused by the competition between the strain energy and the surface energy of the system. The origin of the instability can be related to the reduction of the total free energy of the epitaxial system.

The nanowire ends have a larger adatom concentration than surrounding structures and have, therefore, a concentration gradient that causes adatoms to evolve to larger structures with low adatom concentration. As the nanowire end radius decreases, its adatom concentration increases, increasing similarly the nanowire decay rate [46]. This causes narrow nanowires to decay faster than wide nanowires. Also, similar to their growth, nanowires decay preferentially from the ends.

By studying the time dependence of the average island area during ripening, Bartelt et al. [42] showed that the linear increase or decrease is consistent with detachment-limited kinetics. The linear decay shown in Fig. 10 would suggest that the attachment/detachment-limited kinetics is the dominant decay mechanism for these nanowires [47]. Furthermore, the decay rate apparently decreases significantly at some point. Kodambaka et al. have also observed an abrupt decrease in island decay rates, irrespective of temperature of adatom islands with areas less than a certain critical value. They attribute the size-dependent island decay behavior, which is consistent with detachment-limited kinetics, to anisotropic attachment and detachment barriers [48].

### Hexagonal $DySi_{2-x}$ on Si(111)

Hexagonal $DySi_{2-x}$ is the only phase of the silicide that is reported to form on Si(111) [7, 37, 49, 50]. The epitaxial relationship of hexagonal $DySi_{2-x}$ with Si(111) is [10−10] $RESi_{2-x}$||[−1−12]Si and (0001)$RESi_{2-x}$||(111)Si, and the $DySi_{2-x}$ lattice constants $a = b = 3.83$ Å correspond to a mismatch of −0.26 % in directions parallel with the substrate surface. Therefore, the lattice mismatch for this system is isotropic with an equally small amount of strain in each direction [7, 37]. Although high-quality epitaxial dysprosium silicide films have been reported on Si(111), a minimization of the film's surface and interface energies during the high temperature anneal to 950–1050 °C drives the island formation [25, 26]. Furthermore, the isotropic nature of the system along with the three-fold symmetry of the Si(111) substrate results in the triangular shaped islands that are observed in Figs. 6 and 7 [51].

As shown in Fig. 7a, b, as the sample is annealed at 1050 °C many of the small islands disappear, and the larger islands grow. This is due to the same process of Ostwald ripening that occurs between the nanostructures on Si(001). Moreover, during the deposition of Dy at 1050 °C, only the large island grows from the incident flux (Fig. 7c, d). The size of the smaller nearby island does not change. This can be attributed to the G–T relation which implies that there is a lower adatom concentration at the perimeter of the large island compared to that of the small island. Thus, a concentration gradient exists between the two islands that drive the diffusing adatoms toward the larger island. In addition, because the Dy deposition rate is low, no new nanostructures are detected during this deposition as there were during the deposition displayed in Fig. 4. The low incident flux of Dy allows the atoms sufficient time to diffuse on the surface and attach to preexisting nanostructures before forming critical nuclei with other diffusing adatoms.

An interesting aspect of the growth of the large island in Fig. 7 is that the overall extent of the island does not increase significantly during its growth. Instead, each side of the island grows until all of the kinks are filled in, and a nearly equilateral structure is formed (Fig. 7d). In Fig. 7c, two sides of the island have become completely straight and kink-free after 270 s of Dy deposition. After an additional 290 s of deposition the third side has completely grown out. The incoming Dy flux covers the entire sample surface, so atoms are being deposited near all sides of the island. Despite this, during the time between Fig. 7c and d only one side (the kinked side) of the island grows. This suggests that there is significant adatom diffusion around and/or through the island to the kinked edge. The kinked edge of the island may have an increased surface and interface energy with respect to the kink-free edges. The minimization of this energy may be what drives the adatoms to preferentially diffuse and attach to this portion of the island.

## Summary

The growth and coarsening dynamics of $DySi_{2-x}$ nanostructures on Si(001) and (111) were investigated using in situ, real-time UV PEEM. The deposition of Dy at room temperature followed by annealing to 950–1050 °C resulted in the formation of rectangular silicide nanostructures on Si(001) and triangular silicide nanostructures on Si(111). The nanostructures were observed to grow during continuous annealing via the Ostwald ripening coarsening mechanism, and different growth rates of the individual islands were attributed to local variations in the size and relative location of the surrounding islands on the surface. An abrupt deposition of Dy onto Si(001) at 1050 °C resulted in the growth of the preexisting islands as well as the formation of new island and nanowire structures. Immediately following the deposition, the wires began to decay in favor of the larger, more stable rectangular islands. AFM images indicated that the nanowires have a triangular cross-section, while the rectangular islands have a flat-topped trapezoidal cross-section, and the shape evolution of the nanostructures is related to strain relaxation. A low continuous flux of Dy onto Si(111) at 1050 °C leads

kinks in the larger islands to fill in, resulting in straight-edged, nearly equilateral triangular islands.

**Acknowledgements** This work was supported by the NSF under Grants DMR-0512591 and DMR-0805353 and the AFOSR through the MFEL program. Partial funding for AS-M was provided by U.S. Nuclear Regulatory Commission (Award Number NRC-27-10-1117). We acknowledge the Duke Free Electron Laser Laboratory for access to the OK-4 UV free electron laser. The experimental measurements were completed while AS-M, MCZ, and RJN were at North Carolina State University.

## References

1. Baglin JEJ, d'Heurle FM, Petersson CS (1980) The formation of silicides from thin films of some rare-earth metals. Appl Phys Lett 36:594–596
2. Koleshko VM, Belitsky VF, Khodin AA (1986) Thin-films of rare-earth-metal silicides in microelectronics. Vacuum 36:669–676
3. Tu KN, Thompson RD, Tsaur BY (1981) Low Schottky-barrier of rare-earth silicide on *n*-Si. Appl Phys Lett 38:626–628
4. Norde H, deSousa Pires J, d'Heurle F, Pesavento F, Petersson S, Tove PA (1981) The Schottky-barrier height of the contacts between some rare-earth-metals (and silicides) and *p*-type silicon. Appl Phys Lett 38:865–867
5. Chou Y-C, Lu K-C, Tu KN (2010) Nucleation and growth of epitaxial silicide in silicon nanowires. Mater Sci Eng R 70:112–125
6. Nogami J, Liu BZ, Katkov MV, Ohbuchi C, Birge NO (2001) Self-assembled rare-earth silicide nanowires on Si(001). Phys Rev B 63:233305
7. Knapp JA, Picraux ST (1986) Epitaxial-growth of rare-earth silicides on (111) Si. Appl Phys Lett 48:466–468
8. Luo CH, Shen GH, Chen LJ (1997) Vacancy ordering structures in epitaxial RESi2-*x* thin films on (111)Si and (001)Si. Appl Surf Sci 113(114):457–461
9. Netzer FP (1995) Rare-earth overlayers on silicon. J Phys 7:991–1022
10. Preinesberger C, Vandre S, Kalka T, Dahne-Prietsch M (1998) Formation of dysprosium silicide wires on Si(001). J Phys D 31:L43–L45
11. Chen Y, Ohlberg DAA, Williams RS (2002) Nanowires of four epitaxial hexagonal silicides grown on Si(001). J Appl Phys 91:3213–3218
12. Cui Y, Chung J, Nogami J (2012) Controlling the width of self-assembled dysprosium silicide nanowires on the Si(001) surface. J Phys 24:045003
13. Qui D, Zhang MX, Kelly PM (2009) Crystallography of self-assembled $DySi_2$ nanowires on a Si substrate. Appl Phys Lett 94:083105
14. Eames C, Reakes M, Tear SP, Noakes CQ, Bailey P (2010) Phase selection in the rare earth silicides. Phys Rev B 82:174112
15. Shinde A, Wu R, Ragan R (2010) Thermodynamic driving forces governing assembly of disilicide nanowires. Surf Sci 604:1481–1486
16. Chen Y, Ohlberg DAA, Medeiros-Ribeiro G, Chang YA, Williams RS (2002) Growth and evolution of epitaxial erbium disilicide nanowires on Si (001). Appl Phys A 75:353–361
17. Lee YK, Fujimura N, Ito T, Itoh N (1993) Epitaxial growth and structural characterization of erbium silicide formed on (100) Si through a solid phase reaction. J Cryst Growth 134:247–254
18. Liu BZ, Nogami J (2003) An STM study of dysprosium silicide nanowires on Si(001). J Appl Phys 93:593–599
19. Liu BZ, Nogami J (2003) Growth of parallel rare earth silicide nanowire arrays on vicinal Si(001). Nanotechnology 14:873–877
20. He Z, Smith DJ, Bennett PA (2004) Faulted surface layers in dysprosium silicide nanowires. Phys Rev B 70:241402–241405
21. Chen Y, Ohlberg DAA, Medeiros-Ribeiro G, Chang YA, Williams RS (2000) Self-assembled growth of epitaxial erbium disilicide nanowires on silicon (001). Appl Phys Lett 76:4004–4006
22. Ade H, Yang W, English SL, Hartman J, Davis RF, Nemanich RJ, Litvinenko VN, Pinayev IV, Wu Y, Madey JMJ (1998) A free electron laser–photoemission electron microscope system (FEL–PEEM). Surf Rev Lett 5:1257–1268
23. Nikolic MV, Radic SM, Minic V, Ristic MM (1996) The dependence of the work function of rare earth metals on their electron structure. Microelectron J 27:93–96
24. Allen FG, Gobeli GW (1962) Work function, photoelectric threshold, and surface states of atomically clean silicon. Phys Rev 127:150–158
25. Zinke-Allmang M, Feldman LC, Grabow MH (1992) Clustering on surfaces. Surf Sci Rep 16:377–463
26. Zinke-Allmang M (1999) Phase separation on solid surfaces: nucleation, coarsening and coalescence kinetics. Thin Solid Films 346:1–68
27. Shinde A, Cao J, Lee S, Wu R, Ragan R (2008) An atomistic view of structural and electronic properties of rare earth ensembles on Si(001) substrates. Chem Phys Lett 466:159–164
28. Lee S, Shinde A, Ragan R (2009) Morphological work function dependence of rare-earth disilicide metal nanostructures. Nanotechnology 20:035701
29. Yoshikawa T, Morita K, Kawanishi S, Tanaka T (2010) Thermodynamics of impurity elements in solid silicon. J Alloys Compd 490:31–41
30. Ren FYG, Michel J, Sun-Paduano Q, Zheng B, Kitagawa H, Jacobson DC, Poate JM, Kimerling LC (1993) Ic compatible processing of Si: Er for optoelectronics. Mater Res Soc Symp Proc 298:415–423
31. Tang YS (1991) Enhanced 1.54 μm emission of erbium implanted silicon. Phys Lett A 155:219–221
32. Travlos A, Salamouras N, Boukos N (2003) Growth of rare earth silicides on silicon. J Phys Chem Solids 64:87–93
33. Ye G, Nogami J (2006) Dysprosium disilicide nanostructures on Si(001) studied by scanning tunneling microscopy and transmission electron microscopy. Thin Solid Films 497:48–52
34. Ye G, Crimp MA, Nogami J (2006) Crystallographic study of self-assembled dysprosium silicide nanostructures on Si(001). Phys Rev B 74:033104
35. Ye G, Crimp MA, Nogami J (2009) Self-assembled Gd silicide nanostructures grown on Si(001). J Appl Phys 105:104304
36. Yang J, Cai Q, Wang X-D, Koch R (2004) Morphological evolution of erbium disilicide nanowires on Si(001). Surf Interface Anal 36:104–108
37. Travlos A, Salamouras N, Boukos N (2001) Epitaxial dysprosium silicide films on silicon: growth, structure and electrical properties. Thin Solid Films 397:138–142
38. Tu K, Mayer JW, Feldman LC (1992) Electronic thin film science. Macmillan, New York
39. Jesson DE, Chen G, Chen KM, Pennycook SJ (1998) Self-limiting growth of strained faceted islands. Phys Rev Lett 80:5156–5159
40. Fitting L, Ware ME, Haywood JR, Walter JH, Nemanich RJ (2005) Self-organized nanoscale Ge dots and dashes on SiGe/Si superlattices. J Appl Phys 98:024317
41. Kastner M, Voigtlander B (1999) Kinetically self-limiting growth of ge islands on Si(001). Phys Rev Lett 82:2745–2748
42. Bartelt NC, Theis W, Tromp RM (1996) Ostwald ripening of two-dimensional islands on Si(001). Phys Rev B 54:11741–11751
43. Muller P, Kern R (2000) Equilibrium nano-shape changes induced by epitaxial stress (generalised Wulf–Kaishew theorem). Surf Sci 457:229–253

44. Goldfarb I, Cohen-Taguri G, Grossman S, Levinshtein M (2005) Equilibrium shape of titanium silicide nanocrystals on Si(111). Phys Rev B 72:075430
45. Yang W-C, Ade H, Nemanich RJ (2004) Shape stability of $TiSi_2$ islands on Si (111). J Appl Phys 95:1572–1576
46. Porter DA, Easterling KE (1992) Phase transformations in metals alloys, 2nd edn. Chapman & Hall, London
47. McLean JG, Krishnamachari B, Peale DR, Chason E, Sethna JP, Cooper BH (1997) Decay of isolated surface features driven by the Gibbs–Thomson effect in an analytic model and a simulation. Phys Rev B 55:1811–1823
48. Kodambaka S, Petrova V, Khare SV, Gall D, Rockett A, Petrov I, Greene JE (2002) Size-dependent detachment-limited decay kinetics of two-dimensional TiN islands on TiN(111). Phys Rev Lett 89:176102
49. Vandre S, Kalka T, Preinesberger C, Dahne-Prietsch M (1999) Epitaxial growth and electronic structure of lanthanide silicides on *n*-type Si(111). J Vac Sci Technol B 17:1682–1690
50. He Z, Smith DJ, Bennett PA (2005) Epitaxial $DySi_2$ nanowire formation on stepped Si(111). Appl Phys Lett 86:143110
51. Arnaud d'Avitaya F, Perio A, Oberlin J-C, Campidelli Y, Chroboczek JA (1989) Fabrication and structure of epitaxial Er silicide films on (111) Si. Appl Phys Lett 54:2198–2200